

gram measurements during short-term memory tasks are described by L. Kaufman, S. Curtis, J. Z. Wang, and S. J. Williamson [*Electroencephalogr. Clin. Neurophysiol.* **82**, 266 (1992)] and M. Fahle, J. Albrecht, H. Bueithoff, and D. Braun [*Soc. Neurosci. Abstr.* **20**, 319 (1994)].

22. K. Nakamura, A. Mikami, K. Kubota, *Neuroreports* **3**, 117 (1992).

23. Pyramidal cells are modeled as identical integrate-and-fire neurons. The membrane potential for each pyramidal cell is given by

$$\tau_v dV_i(t)/dt = -V_i(t) + V_{rest} + V_{osc}(t) + V_i^{ADP}(t) + V_i^{inh}(t)$$

and it is reset to $V_{rest} = -60$ mV when it exceeds

$V_{threshold} = -50$ mV, the threshold for spike generation. Because it does not change the qualitative features of the model, we assume that τ_v is small compared to any other time constant, so that

$$V_i(t) \approx V_{rest} + V_{osc}(t) + V_i^{ADP}(t) + V_i^{inh}(t)$$

The inhibitory interneuron is not explicitly modeled; it is activated by each spike in a pyramidal cell and it inhibits all pyramidal cells. This inhibition is assumed to be a linear superposition of inhibitory postsynaptic potentials, such that $V_i^{inh}(t) = \sum \alpha(t - t_n)$, where t_n is the time of the n th spike in the network and α is the alpha function, $\alpha(t) = A^*(t/\tau)^n \exp(-t/\tau)$, with $A^{inh} = -4$ mV and $\tau^{inh} = 5$ ms. V_i^{ADP} increases from zero after each action

potential in cell i (17) with an alpha function of amplitude $A^{ADP} = 10$ mV and a time constant of $\tau^{ADP} = 200$ ms. The oscillatory input is $V_{osc}(t) = B^* \sin(2\pi ft)$, with $f = 6$ Hz and $B = 5$ mV. A memory is inserted through informational inputs at a single negative peak of the cycle. The brief input is sufficient to activate the cells and evoke an ADP.

24. H. S. Obery, *Am. J. Psychol.* **40**, 295 (1928).

25. Supported by the W. M. Keck Foundation and NIH grant NS27337. We thank L. Abbott, S. Sternberg, G. Buzsaki, and M. Kahana for extensive discussions. We extend special thanks to R. Llinas for pointing out Miller's work on memory limits.

13 September 1994; accepted 5 January 1995

TECHNICAL COMMENTS

Interhelical Angles in the Solution Structure of the Oligomerization Domain of p53: Correction

We recently presented the solution structure of the oligomerization domain (residues 319–360) of the tumor suppressor p53 using an multidimensional heteronuclear-edited and -filtered nuclear magnetic resonance (NMR) spectroscopy (1). The structure comprised a dimer of dimers, each dimer being formed by two antiparallel helices and an antiparallel β sheet. The two dimers were arranged approximately orthogonal to each other such that the tetramer formed a four-helical bundle with the antiparallel β sheets lying on opposing faces of the molecule. After the determination of the NMR structure, the crystal structure of the oligomerization domain was solved by Nikola Pavletich and his colleagues and kindly provided to us for comparison (2). While the overall topology of the tetramer was the same in the NMR and x-ray structures, a difference in the orientation of the two dimers (that is between the AC dimer and the BD dimer) was observed. Specifically, the angle between the long axes of helices A and B was 114° in the solution structure versus 80° in the crystal structure. Thus, while the structure of the dimer was similar, the root-mean-square (rms) difference between our proposed NMR structure and the x-ray structure for the complete tetramer was large (3 Å). This difference involves a rigid body rotation of one dimer relative to the other about the symmetry axis of the tetramer and is readily appreciated from the ribbon diagrams of the original NMR structure and the x-ray structure (Fig. 1, A and B, respectively). It is important to determine whether a genuine difference between solution and crystal structures exists, or whether a misinterpretation of the NMR data could

be the cause of this discrepancy.

To this end, we reexamined our nuclear Overhauser enhancement (NOE) data obtained from both the four-dimensional (4D)

$^{13}\text{C}/^{13}\text{C}$ -separated and three-dimensional (3D) ^{13}C -separated/ ^{12}C -filtered NOE spectra. We found that, although the partitioning of the intersubunit NOEs was correct, there were three errors in NOE assignments involving contacts between the A and B subunits (and by symmetry between the C and D subunits). Specifically, the weak NOEs between $\text{Lys}^{351}\text{CeH(A)}$ and $\text{Met}^{340}\text{CyH(B)}$, $\text{Lys}^{351}\text{C}\delta\text{H(A)}$ and $\text{Met}^{340}\text{CaH(B)}$, and $\text{Lys}^{351}\text{CyH(A)}$ and $\text{Met}^{340}\text{CaH(B)}$, which were only identified in the 4D $^{13}\text{C}/^{13}\text{C}$ -separated NOE spectrum, were a

Fig. 1 (right). Ribbon diagrams of (A) the original average NMR structure, (B) the x-ray structure, and (C) the new average NMR structure (3). The angle between helices A and B, which describes the orientation of the two dimers, is 114° in (A), 80° in (B), and 78° in (C). The figure was generated with the program MOLSCRIPT (7).

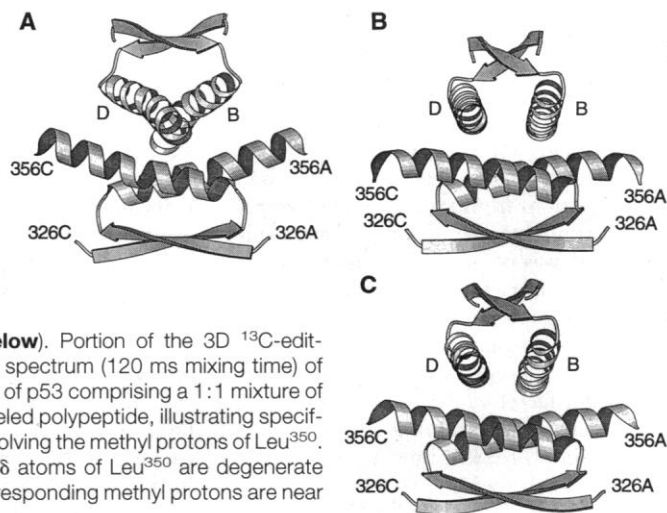
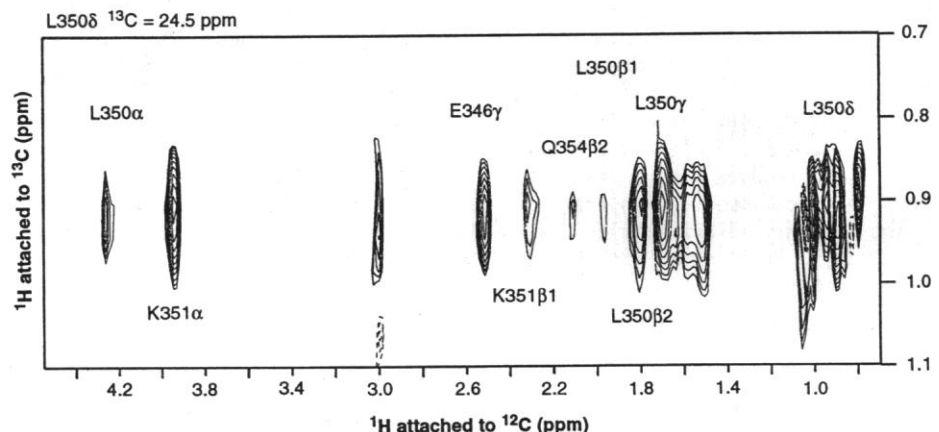


Fig. 2 (below). Portion of the 3D ^{13}C -edited(F_2)/ ^{12}C -filtered(F_3) NOE spectrum (120 ms mixing time) of the oligomerization domain of p53 comprising a 1:1 mixture of unlabeled and $^{13}\text{C}/^{15}\text{N}$ -labeled polypeptide, illustrating specifically intersubunit NOEs involving the methyl protons of Leu^{350} . The ^{13}C shift of the two $\text{C}\delta$ atoms of Leu^{350} are degenerate and the ^1H shifts of the corresponding methyl protons are near degenerate.



result of spectral artifacts. Also, key intersubunit NOEs between helices A and B involving the methyl groups of Leu³⁵⁰CδH had been omitted from the NOE restraints list. These included a strong NOE from Leu³⁵⁰-CδH(A) to Lys³⁵¹CαH(B), as well as weak NOEs to Lys³⁵¹Cβ1H(B) and Gln³⁵⁴-Cβ2H(B) (Fig. 2). Even when the three incorrect NOEs were omitted and the structures recalculated, the orientation of the two dimers differed by 25° from that in the crystal structure. Introduction of the new NOEs, however, fully corrected this situation, as can be seen from the ribbon diagram of the new average NMR structure (Fig. 1C) (3).

As a result of these corrections, the difference between the average backbone coordinates of the new ensemble of NMR structures and the crystal structure for the residues visible in the electron density map is 1.2 Å for the whole tetramer. The precision of the NMR backbone coordinates is 0.45 Å which, assuming no errors in the experimental restraints, translates into a mean coordinate accuracy of 0.9 to 1.1 Å (4). Hence, the two structures are essentially identical within the errors of the present NMR coordinates.

It is instructive to examine the source of the errors in our earlier study (1). Conventionally, in a single chain protein, errors in NOE assignments manifest themselves by inconsistencies. In this particular case, this was not evident, as excellent agreement between the calculated and input values of the NOE, torsion and coupling constant restraints, good nonbonded contacts, and small deviations from idealized covalent geometry, were obtained. Complete cross-validation (5) was of little help, as it did not result in a significant change in the structure because the target function also incorporated symmetry restraints. Finally, the fourfold degeneracy reduced the number of unique NOEs by a factor of 4, thereby increasing the difficulty in ascertaining errors.

Why were three key intersubunit NOEs, Leu³⁵⁰CδH(A) to Lys³⁵¹CαH(B), Lys³⁵¹-Cβ1H(B) and Gln³⁵⁴Cβ2H(B), omitted from the restraint list, and why did their omission result in a large reorientation of the two dimers? First, the problem with our proposed structure reflected to some extent the limitation of the NMR technique itself, as the main structural parameter, and the only one involved in determining long-range order, involves short (<5 Å) interproton distances derived from the NOEs. As the number of observed NOEs between

the A and B dimers is limited to 24, propagation of errors can easily occur. This may have been further compounded by our representing the nonbonded contacts by only a repulsive term, which worked to reduce the contact area between the two dimers. Second, two of the crucial NOEs involve two neighboring residues for which intrasubunit NOEs would occur, although in the 3D ¹³C-edited/¹²C-filtered NOE spectrum carried out on the unlabeled-labeled heterotetramer, these should not be observable. We noticed, however, experimental problems with this spectrum. For example, strong cross peaks were observed from the methyl protons of Ala³⁵³ and Ala³⁵⁵ to their respective CαH protons despite the fact that the intersubunit separation between these two proton pairs was more than 14 Å. Consequently, we attributed these peaks to artifacts arising from intrasubunit NOEs, possibly as a result of incomplete ¹³C labeling. The Leu³⁵⁰CδH to Lys³⁵¹CαH and Lys³⁵¹Cβ1H peaks were thought to reflect a similar situation. Third, in a single-chain protein, the angle between structural elements corresponding to the two dimers would also be restricted by the limitations imposed by covalent geometry. Last, in a contiguous single polypeptide chain, the three crucial NOEs would correspond to 12 unique NOEs.

The reason for the profound effect of these additional restraints lies to some degree in the orthogonal packing of the two dimers. The large majority of NOE restraints are at the center of the helices, whereas many of those involving Leu³⁵⁰-CδH lie at the end of the helices, thereby exerting more leverage on the overall interhelix orientation.

What are the consequences of the correction in angle between the two dimers? First, the overall topology of the tetramer remains the same, and the main thrust and conclusions of our article (1) are unaffected. From a structural viewpoint, however, the packing of the two dimers is slightly better in the new NMR structure and in the crystal structure than in the one we proposed originally (1).

After the submission of this comment, Lee *et al.* (6) also published an NMR structure of the oligomerization domain. The angle between helices A and B in this structure was 55° to 60° [figure 8D in (6)] compared with 80° and 78° in the x-ray and new NMR structures, respectively, and 114° in the original NMR structure. This illustrates the high degree of technical difficulty

in solving the structure of this symmetrical homotetramer by NMR.

G. Marius Clore

James G. Omichinski

Laboratory of Chemical Physics,
National Institute of Diabetes and
Digestive and Kidney Diseases,
National Institutes of Health,
Bethesda, MD 20892, USA

Kazuyasu Sakaguchi

Nicola Zambrano

Hiroshi Sakamoto

Ettore Appella

Laboratory of Cell Biology,
National Cancer Institute,
National Institutes of Health,
Bethesda, MD 20892, USA

Angela M. Gronenborn

Laboratory of Chemical Physics,
National Institute of Diabetes and Digestive
and Kidney Diseases

REFERENCES AND NOTES

1. G. M. Clore *et al.*, *Science* **265**, 386 (1994).
 2. P. D. Jeffrey, S. Gorina, N. P. Pavletich, *ibid.* **267**, 1498 (1995). N. P. Pavletich, personal communication.
 3. The structural statistics are as follows: A total of 35 simulated annealing structures were calculated as described in (1) on the basis of a total of 3268 approximate interproton distance restraints comprising 2404 intrasubunit restraints (744 intraresidue, 844 sequential $i - j = 1$, 744 medium range $1 < i - j \leq 5$, and 72 long range $i - j > 5$ restraints) and 864 intersubunit restraints (758 for the AC and BD dimers, 96 for the AB and CD dimers, and 10 for the AD and BC dimers), supplemented by 128 distance restraints for 64 intrasubunit hydrogen bonds, 24 distance restraints for 12 intersubunit hydrogen bonds, 144 ³JH_Nα coupling constant restraints, and 268 torsion angle restraints (144 φ, 104 χ₁, and 20 χ₂). The precision of the structures (defined as the average atomic rms difference between the individual
- all atoms for residues 326 to 356. (Residues 319–325 at the NH₂-terminus and 357–360 at the COOH-terminus are disordered in solution.) The rms deviations from the experimental restraints are as follows: 0.053 ± 0.003 Å, 0.27 ± 0.02 Hz, and 0.23 ± 0.15°, for the distance, coupling constant, torsion angle, Cα shift, and Cβ shift restraints, respectively. The deviations for idealized covalent geometry are 0.002 ± 0.0001 Å, 0.446 ± 0.010°, and 0.335 ± 0.069° for bond, angle, and improper torsion terms. The coordinates of the 35 simulated annealing structures, and those of the restrained regularized mean structure, together with the experimental NMR restraints and the ¹H, ¹³C, and ¹⁵N chemical shift assignments have been deposited in the Brookhaven Protein Data Bank (accession code numbers 1OLH, 1OLG, and 1OLH.MR, respectively).
4. G. M. Clore, M. A. Robien, A. M. Gronenborn, *J. Mol. Biol.* **231**, 82 (1993).
 5. A. T. Brünger *et al.*, *Science* **261**, 328 (1993).
 6. W. Lee *et al.*, *Nature Struct. Biol.* **1**, 877 (1994).
 7. P. J. Kraulis, *J. Appl. Crystallogr.* **24**, 946 (1991).

16 November 1994; accepted 9 January 1995